Journal of Alloys and Compounds 505 (2010) 101–107

Contents lists available at ScienceDirect

Journal of Alloys and Compounds

journal homepage: www.elsevier.com/locate/jallcom

The $CuInSe_2$–$CuGaSe_2$–2CdSe system and crystal growth of the γ-solid solutions

L.P. Marushko[a,*], Y.E. Romanyuk[b], L.V. Piskach[a], O.V. Parasyuk[a], I.D. Olekseyuk[a], S.V. Volkov[c], V.I. Pekhnyo[c]

[a] Department of General and Inorganic Chemistry, Volyn National University, Voli Ave 13, Lutsk 43009, Ukraine
[b] Swiss Federal Laboratories for Materials Testing and Research, EMPA, Überlandstrasse 129, CH-8600 Dübendorf, Switzerland
[c] V.I. Vernadskii Institute for General and Inorganic Chemistry of the Ukrainian National Academy of Sciences, Palladina Ave 32-34, Kyiv 03680, Ukraine

ARTICLE INFO

Article history:
Received 10 March 2010
Received in revised form 4 June 2010
Accepted 9 June 2010
Available online 18 June 2010

Keywords:
Semiconductors
Crystal growth
Phase diagrams
Thermal analysis
X-ray diffraction

ABSTRACT

Phase equilibria in the $CuInSe_2$–$CuGaSe_2$–2CdSe system are studied using differential-thermal analysis and phase X-ray diffraction. An isothermal section of the system at 870 K, and phase diagrams of polythermal sections $CuInSe_2$–$CuGaSe_2$ and '$CuCd_2InSe_4$'–$CuCd_2GaSe_4$ have been constructed. The '$CuCd_2InSe_4$'–$CuCd_2GaSe_4$ section is not quasi-binary and includes two solid solution regions with the wurtzite and sphalerite structure-types. Eleven crystals of the γ-solid solutions with the sphalerite structure-type were grown by the Bridgman technique. The non-quasi-binary nature of the '$CuCd_2InSe_4$'–$CuCd_2GaSe_4$ section gives rise to compositional gradients for copper, cadmium, and gallium along the crystal growth direction so that the crystal tip is enriched with CdSe. Band gap of the grown crystals varies from 1.05 eV to ~1.30 eV.

1. Introduction

Ternary chalcopyrite compounds $CuInSe_2$, $CuInS_2$, and $CuGaSe_2$ are considered as alternative materials to silicon for thin film solar cell applications [1–3]. These compounds are readily obtained with the p-type conductivity and, in combination with the n-type CdS, can form the p–n heterojunction necessary for the separation of photo-generated carriers. A remarkable property of chalcopyrites is their ability to form solid solutions, $CuInS_xSe_{2-x}$ [4,5], $CuIn_xGa_{1-x}Se_2$ [1,2,6], $CuIn_xGa_{1-x}S_ySe_{2-y}$ [1,7,8], etc., which not only allow tuning the semiconductor band gap to achieve the maximum photoconversion efficiency but also ensure the observed high tolerance to compositional variations. In this respect, the investigation of phase relations between ternary chalcopyrites together with other II–VI compounds is important to assess possible element interdiffusion at the p-n heterojunction and to extend the knowledge about solid solutions and possible intermediate phases.

In previous studies we investigated phase relations in ternary systems $CuInS_2 + 2CdSe \leftrightarrows CuInSe_2 + 2CdS$ [9], $CuGaS_2 + 2CdSe \leftrightarrows CuGaSe_2 + 2CdS$ [10], and $CuInS_2$–$CuGaS_2$–2CdS [11], which can be considered as boundary faces of the quaternary exchange system (CuIn),(CuGa),Cd//S,Se. Intermediate solid solution, called the γ-phase, exists in the $CuInS_2 + 2CdSe \Leftrightarrow CuInSe_2 + 2CdS$ system. The γ-phase is based on the high-temperature (HT) modifications of $CuInS_2$ and $CuInSe_2$ with the sphalerite structure-type, which is stabilized at lower temperatures with the addition of CdS or CdSe [9]. Physical properties of the γ-solid solutions were studied on the single crystals grown by the horizontal Bridgman technique [12]. The crystals are photosensitive, mostly of the p-type conductivity, with the hole concentration of 10^{15}–10^{16} cm^{-3} and the Hall mobility of 18 cm/(V × s). The band gap varies in the range from 1.05 eV to 1.43 eV, indicating a potential for solar cell applications. Limited γ-solid solutions with the sphalerite structure-type are also formed around the composition $CuCd_2GaSe_4$ in the $CuGaS_2 + 2CdSe \leftrightarrows CuGaSe_2 + 2CdS$ system [10], as well as in the $CuInS_2$–$CuGaS_2$–2CdS system [11].

In the present study we investigate the quasi-ternary system $CuGaSe_2$–$CuInSe_2$–2CdSe, which is a boundary face of the quaternary exchange system (CuIn),(CuGa),Cd//S,Se, in order to determine the formation of the γ-solid solutions based on the HT sphalerite modification of $CuInSe_2$.

2. Quasi-binary boundary systems

2.1. System $CuGaSe_2$–CdSe

The $CuGaSe_2$–CdSe system was studied in Refs. [13–15]. The intermediate compound $CuCd_2GaSe_4$ exhibits a polymorphous

* Corresponding author. Tel.: +380 3322 49467; fax: +380 3322 41007.
E-mail address: marushko777@mail.ru (L.P. Marushko).

0925-8388/$ – see front matter © 2010 Elsevier B.V. All rights reserved.
doi:10.1016/j.jallcom.2010.06.053

transformation at 1163 K turning from the low temperature cubic modification (sphalerite, space group $F\bar{4}3m$, lattice constant $a = 0.583$ nm) into the hexagonal HT modification (wurtzite, space group $P6_3mc$, lattice constants $a = 0.410$ nm and $c = 0.673$ nm) [13]. The melting point of $CuCd_2GaSe_4$ is at 1290 K. According to Ref. [14] the room temperature solid solubility is 10 mol.% of $CuGaSe_2$ in CdSe and 1 mol.% of CdSe in $CuGaSe_2$.

The phase diagram of the system was investigated in Ref. [15]. Since $CuGaSe_2$ is formed after the peritectic reaction [16–18], the $CuGaSe_2$–CdSe section is not quasi-binary. The intermediate phase is formed in the system after the peritectic reaction $L + \beta \rightarrow \delta$ at 1320 K. The peritectic horizontal extends from 40 mol.% to 72 mol.% CdSe. Compound $CuCd_2GaSe_4$ is a berthollide phase whose composition corresponds to the formation point of the δ-phase. When annealed at 870 K, it crystallizes with cubic symmetry ($a = 0.5825$ nm), whereas annealing at 1220 K results in the hexagonal crystal system ($a = 0.4141$ nm, $c = 0.6786$ nm), because the composition falls in the range of the β-solid solution based on CdSe. The eutectic point coordinates are 1310 K and 35 mol.% CdSe. The solid solubility at 870 K is 0–7.5 mol.% CdSe for α-solid solution ($CuGaSe_2$), 52–78 mol.% CdSe for δ-solid solution ($CuCd_2GaSe_4$), and 87.5–100 mol.% CdSe for β-solid solution (CdSe).

2.2. System $CuInSe_2$–CdSe

The phase diagram of the $CuInSe_2$–CdSe system was studied in Refs. [19–21]. The system is of the peritectic type with the invariant point at 2 mol.% CdSe at 1260 K according to Ref. [21]. There is a minimum on the liquidus curve near $CuInSe_2$. The point where both the liquidus and the solidus meet is between 1 mol.% and 2 mol.% CdSe. The boundary CdSe β-solid solution shrinks significantly with the temperature decrease and extends to 82–100 mol.% CdSe at 870 K (or 75–100 mol.% 2CdSe [9]). The γ-solid solution, which crystallizes in the sphalerite structure-type, is formed by three ways: directly from the melt in the range of 0–2 mol.% CdSe, as a result of the peritectic reaction in the range of 2–33 mol.% CdSe, and after the decomposition of the β-solid solution. It is stated in Ref. [21] that the quaternary compound reported in Refs. [19,20] is actually the γ-solid solution based on the HT-modification of $CuInSe_2$ stabilized by CdSe. The solubility limits determined from the variation of lattice constants are 26–76 mol.% CdSe at 870 K.

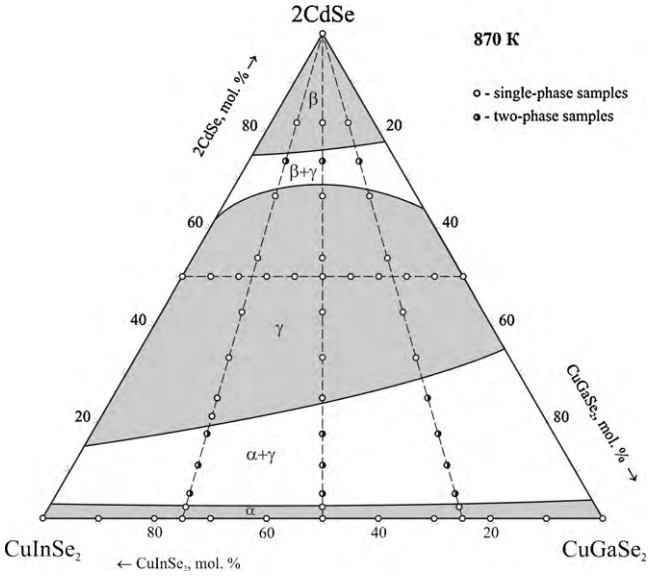

Fig. 1. Chemical and phase compositions of the investigated alloys on the isothermal section of the $CuGaSe_2$–$CuInSe_2$–2CdSe system at 870 K.

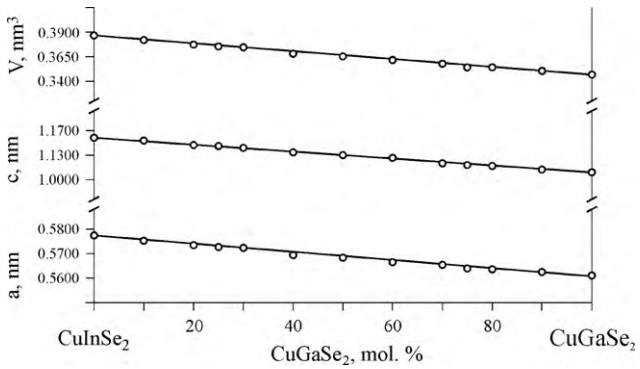

Fig. 2. Variation of the lattice constants for the $CuInSe_2$–$CuGaSe_2$ system.

The α-solid solution has the chalcopyrite structure-type and is found in the range of 0–6 mol.% CdSe at 870 K.

2.3. System $CuInSe_2$–$CuGaSe_2$

The phase diagram of the $CuInSe_2$–$CuGaSe_2$ system was established in [22]. A continuous range of solid solutions is formed between the components, so the phase diagram is referred to type I according to Rozeboom's classification. Two thermal effects are detected for each ternary component, 1318 K and 1361 K for $CuGaSe_2$, and 1083 K and 1259 K for $CuInSe_2$. The phase transitions at 1318 K and 1083 K are interpreted as cation–cation disordering of the crystal structure. Similar phase transformations are observed for all solid solutions $CuGa_xIn_{1-x}Se_2$ in the full concentration range. Single crystals of the $CuGa_xIn_{1-x}Se_2$ solid solutions were grown in Ref. [23]. The crystals have the chalcopyrite structure-type and p-type conductivity. Their lattice constants vary linearly in agreement with Vegard's law.

3. Experimental

For the investigation of phase relations in the $CuGaSe_2$–$CuInSe_2$–2CdSe system, 59 alloys were synthesized with compositions depicted on Fig. 1. Initial charges were

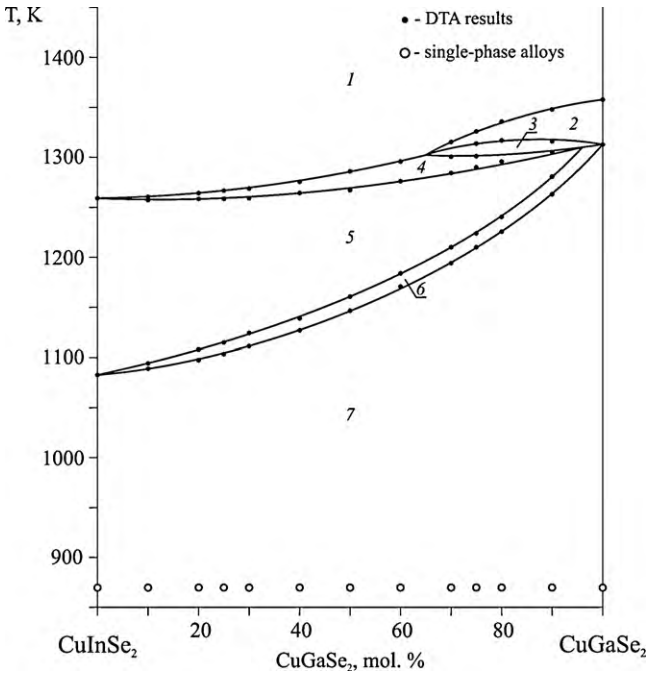

Fig. 3. Polythermal section $CuInSe_2$–$CuGaSe_2$ (1, L; 2, $L + \gamma'$; 3, $L + \gamma' + \gamma$; 4, $L + \gamma$; 5, γ; 6, $\alpha + \gamma$; 7, α).

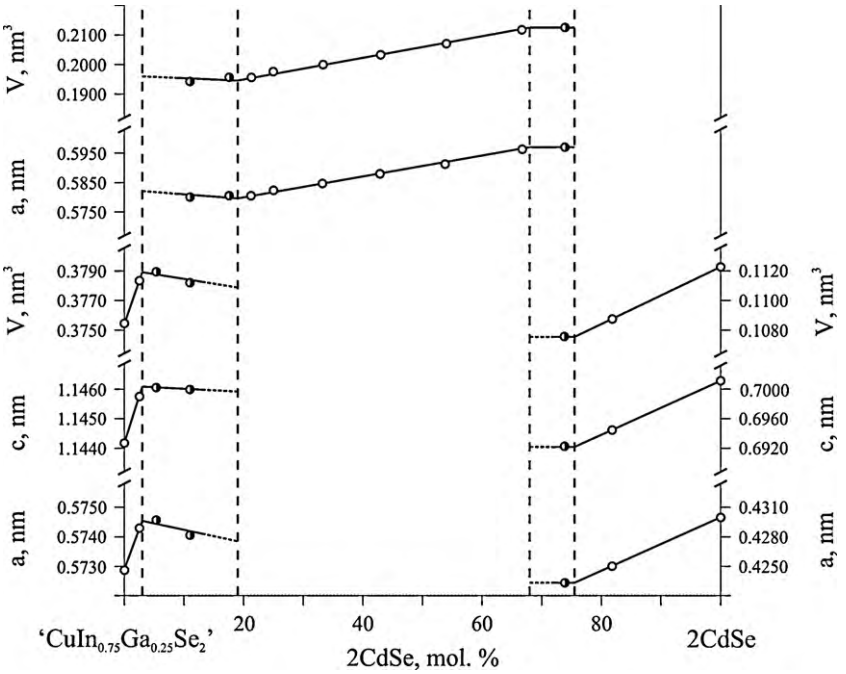

Fig. 4. Variation of the lattice constants for the '$CuIn_{0.75}Ga_{0.25}Se_2$'–2CdSe section.

prepared from individual elements with purity better than 99.99 wt.%. The batches were loaded in quartz ampoules, which were evacuated to 10^{-2} Pa and then soldered up. The synthesis was carried out in a single-zone vertical furnace with a heating rate of 50 K/h. The maximum temperature was 1470 K. After dwelling the melts at the maximum temperature for 2–3 h, they were slowly cooled to 870 K at a rate of 10 K/h. The alloys were annealed for 500 h at that temperature and then quenched in cold water.

Obtained alloys were investigated using differential-thermal analysis (DTA) (Paulik, Paulik, Erdey system [24] with a Pt/Pt–Rh thermocouple) and phase X-ray diffraction (XRD) (diffractometer DRON-4-13, CuK_α radiation). Lattice constants were calculated using software package PDWin-2.

Single crystals of the γ-solid solutions were grown by a horizontal variation of the Bridgman technique in an industrial furnace DN-12. Crystal compositions were selected along the section '$CuCd_2InSe_4$'–$CuCd_2GaSe_4$ with a step of 10 mol.% of $CuCd_2GaSe_4$. Initial batches of 7 g were loaded into graphitized quartz ampoules with conical bottom. The ampoules were evacuated and sealed. The crystal growth consisted of two stages. First, the batches were heated in the flame of an oxygen-gas burner to let the elements react. Next, the alloys were heated to 1470 K in the horizontal furnace inclined at 5–10°, and the melts were homogenized during 4 h by rotating the ampoules by a motor connected to ampoules via a quartz rod. The ampoules were then pulled horizontally at a rate of 1 mm/h. The temperature gradient at the crystallization interface did not exceed 14 K/cm. After reaching the

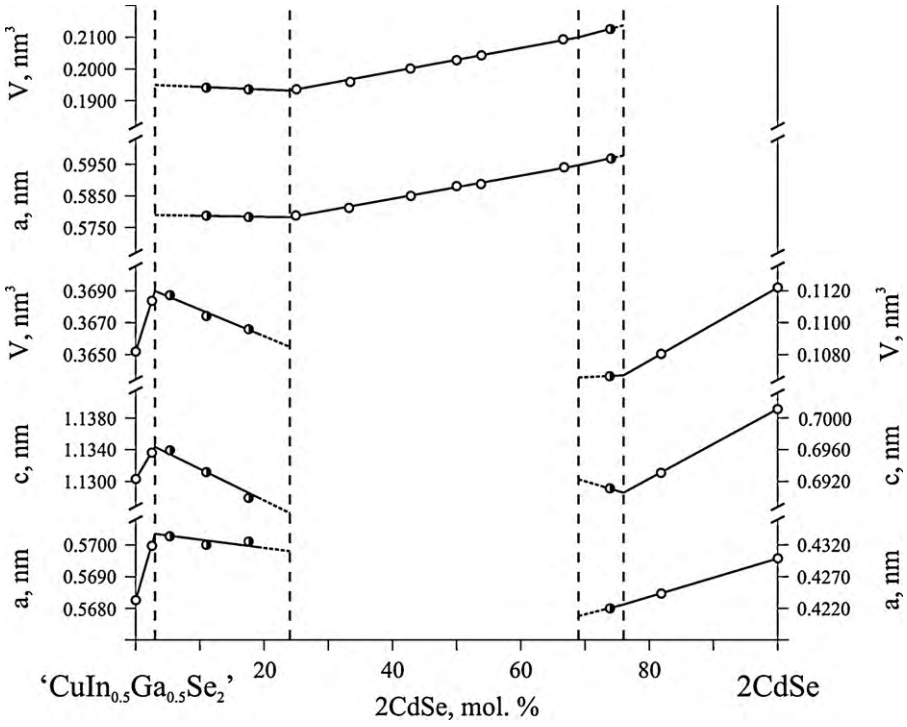

Fig. 5. Variation of the lattice constants for the '$CuIn_{0.5}Ga_{0.5}Se_2$'–2CdSe section.

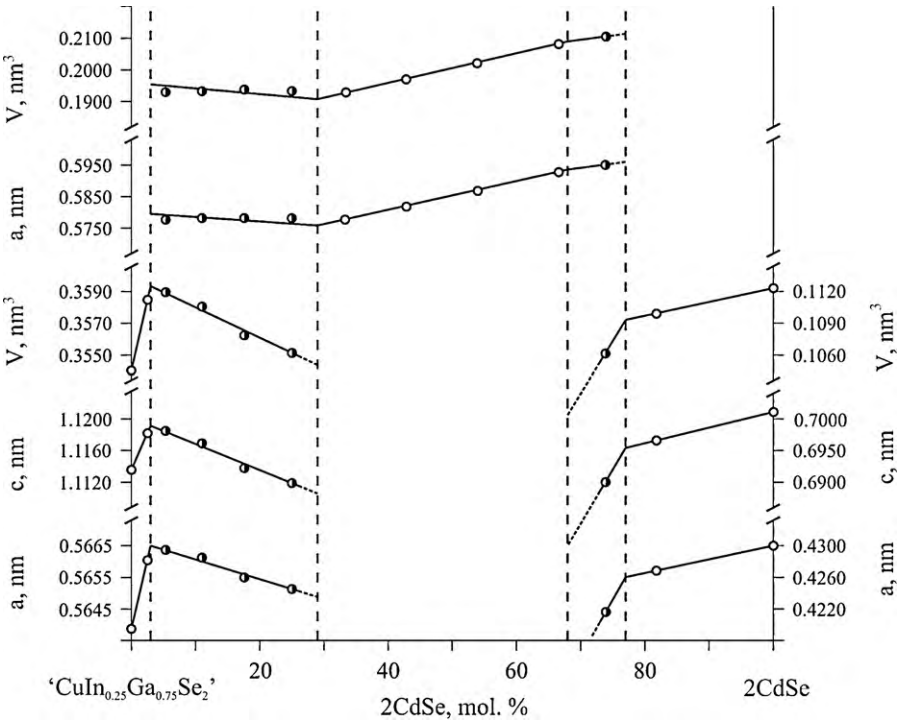

Fig. 6. Variation of the lattice constants for the '$CuIn_{0.25}Ga_{0.75}Se_2$'–2CdSe section.

isothermal zone held at 870 K, the crystals were annealed for 250 h and then cooled to room temperature at a rate of 100 K/day. As a result, we obtained ingots consisting of single crystal blocks with dimensions suitable for physical experiments.

Crystal plates of 2 mm in thickness were cut along the solidification direction and their faces were polished using diamond pastes. Chemical composition at different points of the crystal plates was determined by energy-dispersive X-ray analysis (EDX) on scanning electron microscope Hitachi S-4800 with EDX attachment from Oxford Instruments. An acceleration voltage of 20 kV was applied to monitor K-series lines for Ga, Cu, and Se, and L-series for Cd and In. Quantum optimization on copper reference was performed before measurements. Element quantifications were done with INCA 5.12 package using internal standards.

The band gap of the grown crystals was measured by photomodulated reflectance (PR) spectroscopy at room temperature [25]. The crystal plates were briefly etched in Br_2-ethanol solution in order to remove surface oxides and refresh the surface after the mechanical polishing. Radiation from a 300 W halogen tungsten lamp dispersed by a 0.5 m monochromator was focused on the samples as a probe beam. A chopped He–Cd laser beam at 325 nm provided the photomodulation. PR signals were detected by a Si or Ge photodiode using a phase-sensitive lock-in amplification system.

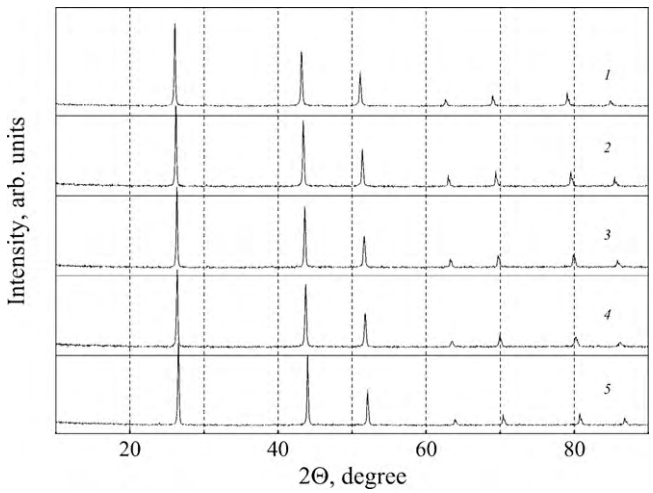

Fig. 7. Selected XRD patterns for alloys of the '$CuCd_2InSe_4$'–$CuCd_2GaSe_4$ section (in mol.% $CuCd_2GaSe_4$): (1) 0, (2) 30, (3) 50, (4) 70, and (5) 100.

4. Results

4.1. Isothermal section of the $CuGaSe_2$–$CuInSe_2$–2CdSe system at 870 K

Fig. 1 presents the isothermal section of the system at 870 K determined from the powder XRD data.

There are three single-phase regions in the system at 870 K. The first is the continuous α-solid solution between $CuGaSe_2$ and $CuInSe_2$ with the chalcopyrite structure-type. The second single-phase region belongs to the β-solid solution based on CdSe with the wurtzite structure-type. The third region is the γ-solid solution with the sphalerite structure-type between the HT-modification of $CuInSe_2$, which is stabilized at the annealing temperature by CdSe, and $CuCd_2GaSe_4$. There are also two two-phase regions containing mixtures α + γ and β + γ.

4.2. System $CuGaSe_2$–$CuInSe_2$

Our powder XRD results confirm the data from [22,23] that all samples of the $CuInSe_2$–$CuGaSe_2$ system are single-phase ones at 870 K. The variation of the lattice constants with the solid solution composition is in agreement with Vegard's law (Fig. 2).

The phase diagram of the $CuInSe_2$–$CuGaSe_2$ system reported in Ref. [22] is not consistent with the fact that $CuGaSe_2$ is formed after a peritectic reaction in the Cu_2Se–Ga_2Se_3 system [16–18]. Therefore, we have re-investigated the system. The constructed phase diagram (Fig. 3) agrees well with the data of [22] in the range of low temperatures. However, there are two additional fields (2 and 3) at liquidus temperatures at the $CuGaSe_2$-rich side, which are caused by the peritectic formation of copper selenogallate.

4.3. Sections '$CuIn_{0.75}Ga_{0.25}Se_2$'–2CdSe, '$CuIn_{0.5}Ga_{0.5}Se_2$'–2CdSe and '$CuIn_{0.25}Ga_{0.75}Se_2$'–2CdSe

The '$CuIn_{0.75}Ga_{0.25}Se_2$'–2CdSe section contains single-phase regions at 0–3 mol.% 2CdSe (α-solid solution), ~76–100 mol.%

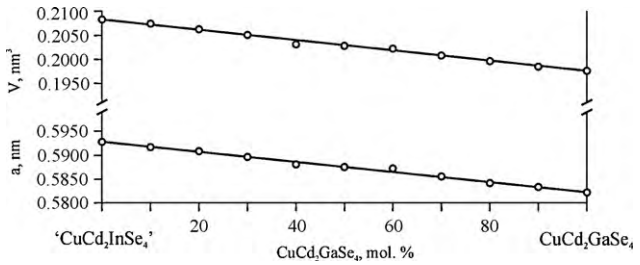

Fig. 8. Variation of the lattice constant along the '$CuCd_2InSe_4$'–$CuCd_2GaSe_4$ section.

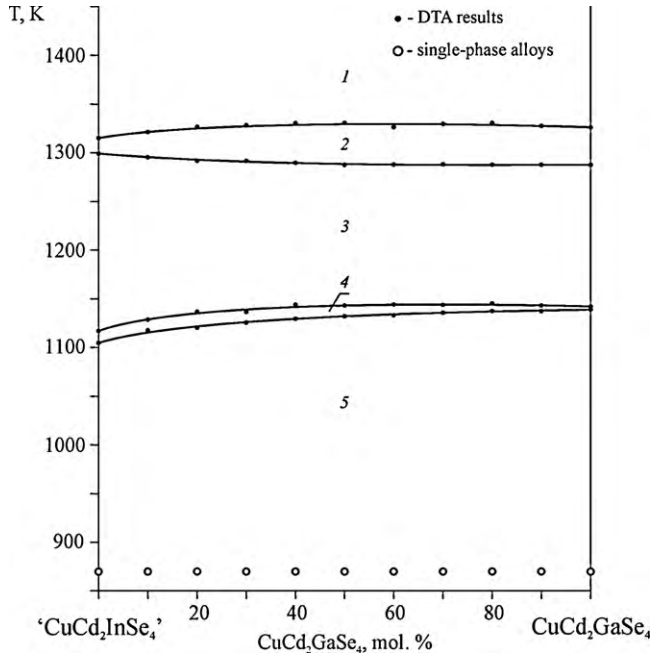

Fig. 9. Polythermal section '$CuCd_2InSe_4$'–$CuCd_2GaSe_4$ (1, *L*; 2, *L* + β; 3, β; 4, β + γ; 5, γ).

2CdSe (β-solid solution) and 19–68 mol.% 2CdSe (γ-solid solution) at the annealing temperature. The variation of the lattice constants is presented in Fig. 4.

Along the '$CuIn_{0.5}Ga_{0.5}Se_2$'–2CdSe section at the annealing temperature the ranges of the solid solutions are 0–3 mol.%, 76–100 mol.%, and 24–69 mol.% 2CdSe for the α-, β-, and γ-solid solutions, respectively. The variation of the lattice constants with the alloy composition is given in Fig. 5.

Along the '$CuIn_{0.25}Ga_{0.75}Se_2$'–2CdSe section at the annealing temperature, the ranges of the solid solutions are 0–3 mol.%,

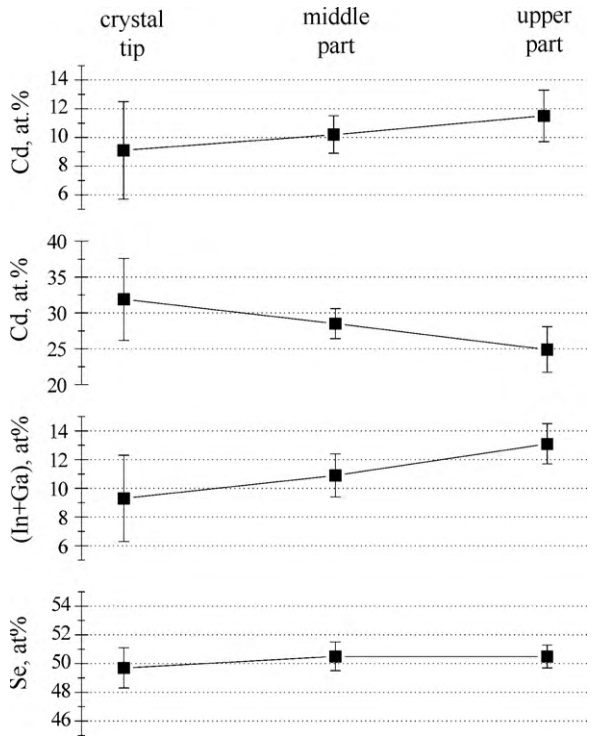

Fig. 11. Variation of the chemical composition along the crystal length. The crystal solidifies starting from the tip. Results for 11 crystals are averaged, and the error bars are respective standard deviations.

77–100 mol.%, and 29–68 mol.% 2CdSe for the α-, β-, and γ-solid solutions, respectively. The variation of the lattice constants with the alloy composition is given in Fig. 6.

According to Vegard's law lattice constant should change linearly in single-phase region and remain constant in two-phase regions. However, a change in the lattice constant is observed even for two-phase regions in Figs. 4–6. This is possible because the considered sections cross conodes (or tie-lines) with different lattice constants in the two-phase regions.

4.4. Section '$CuCd_2InSe_4$'–$CuCd_2GaSe_4$

Typical XRD patterns of the '$CuCd_2InSe_4$'–$CuCd_2GaSe_4$ section are presented in Fig. 7. All samples are single-phase, which is also confirmed by the linear variation of the lattice constants (Fig. 8).

The phase diagram of the '$CuCd_2InSe_4$'–$CuCd_2GaSe_4$ section was constructed in Fig. 9 using the DTA results to select optimum conditions for the crystal growth of the γ-solid solutions.

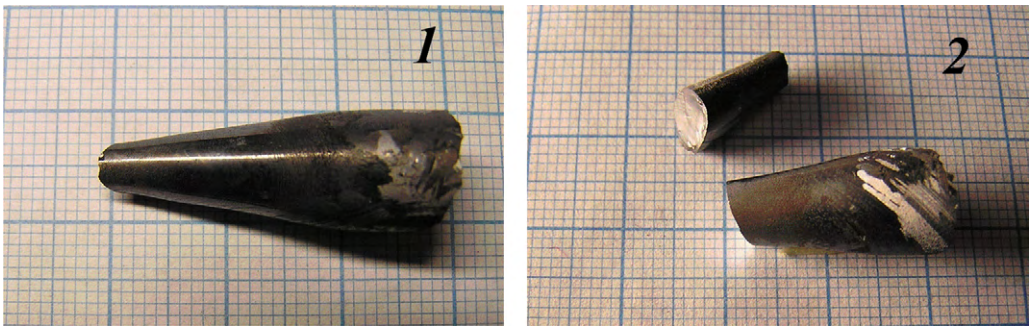

Fig. 10. Two selected crystals of the γ-solid solutions along the '$CuCd_2InSe_4$'–$CuCd_2GaSe_4$ section (in mol.% $CuCd_2GaSe_4$): (1) 90 and (2) 100. The main division of the background scale is 1 cm.

As the temperature decreases, β-solid solutions crystallize first; then they undergo decomposition that results in the formation of γ-solid solutions.

4.5. Crystal growth of the γ-solid solutions and investigation of their properties

The crystals of the γ-solid solutions along the '$CuCd_2InSe_4$'–$CuCd_2GaSe_4$ section were grown by the method described in Section 3. The γ-solid solutions are formed after the decomposition of the β-solid solutions below the solidus line in the $CuInSe_2$–$CuGaSe_2$–2CdSe system, complicating their single crystal growth. Therefore, a prolonged annealing had to be applied. As a result, 11 crystal boules were obtained, and two of them are shown in Fig. 10.

The chemical composition of the crystals measured by EDX is given in Table 1. The composition for each crystal was determined for three points, namely crystal tip, middle part, and upper part. For each investigated crystal, the chemical composition differs for different parts. As it was mentioned earlier, the '$CuCd_2InSe_4$'–$CuCd_2GaSe_4$ section is not a quasi-binary but is a part of the $CuInSe_2$–$CuGaSe_2$–2CdSe system. Taking into account melting points of the system components, one should expect a decrease in the liquidus and solidus temperatures with the reduction of the CdSe content. Therefore, a composition gradient along the growth direction is expected for the γ-solid solutions crystals from the

Table 1
Composition of the grown γ-solid solution crystals along the '$CuCd_2InSe_4$'–$CuCd_2GaSe_4$ section as measured by EDX.

$CuCd_2GaSe_4$, content, mol.%	Element	Calculated concentration, at.%	Measured concentration, at.% with statistical error for peak fitting		
			Part of the crystal		
			Lower (tip)	Middle	Upper
0	Cu	12.5	13.23 ± 0.66	12.28 ± 0.64	13.32 ± 0.65
	Ga	0.0	0.00	0.00	0.00
	Se	50.0	46.96 ± 1.22	49.10 ± 1.19	50.01 ± 1.18
	Cd	25.0	27.53 ± 0.65	25.40 ± 0.63	22.47 ± 0.61
	In	12.5	12.28 ± 0.52	13.22 ± 0.52	14.21 ± 0.52
10	Cu	12.5	9.63 ± 0.60	10.54 ± 0.61	12.11 ± 0.68
	Ga	1.25	0.00	0.00	0.00
	Se	50.0	50.89 ± 1.21	51.35 ± 1.19	50.89 ± 1.26
	Cd	25.0	29.58 ± 0.68	28.9 ± 0.67	26.07 ± 0.67
	In	11.25	9.89 ± 0.51	9.21 ± 0.51	10.92 ± 0.53
20	Cu	12.5	14.06 ± 0.67	11.41 ± 0.65	12.51 ± 0.63
	Ga	2.5	1.33 ± 0.60	0.00	2.78 ± 0.57
	Se	50.0	47.85 ± 1.24	50.1 ± 1.24	49.92 ± 1.17
	Cd	25.0	26.74 ± 0.67	28.33 ± 0.68	23.93 ± 0.60
	In	10	10.02 ± 0.50	10.16 ± 0.52	10.86 ± 0.49
30	Cu	12.5	8.62 ± 0.60	9.68 ± 0.61	11.19 ± 0.60
	Ga	3.75	2.81 ± 0.61	2.08 ± 0.62	3.60 ± 0.60
	Se	50.0	48.90 ± 1.25	51.83 ± 1.23	50.08 ± 1.17
	Cd	25.0	32.05 ± 0.73	28.52 ± 0.69	25.54 ± 0.62
	In	8.75	7.62 ± 0.51	7.9 ± 0.51	9.59 ± 0.49
40	Cu	12.5	7.47 ± 0.35	7.77 ± 0.35	7.61 ± 0.35
	Ga	5.0	2.83 ± 0.37	3.85 ± 0.38	4.64 ± 0.39
	Se	50.0	49.45 ± 1.17	49.86 ± 1.18	49.48 ± 1.17
	Cd	25.0	34.07 ± 0.43	32.52 ± 0.43	30.81 ± 0.42
	In	7.5	6.18 ± 0.37	6.01 ± 0.37	7.46 ± 0.37
50	Cu	12.5	10.13 ± 0.38	11.02 ± 0.38	12.88 ± 0.40
	Ga	6.25	4.80 ± 0.40	5.82 ± 0.41	7.43 ± 0.43
	Se	50.0	49.65 ± 1.19	48.99 ± 1.16	50.77 ± 1.17
	Cd	25.0	29.68 ± 0.41	27.63 ± 0.40	22.79 ± 0.38
	In	6.25	5.75 ± 0.36	6.55 ± 0.35	6.13 ± 0.34
60	Cu	12.5	9.43 ± 0.38	10.07 ± 0.37	12.62 ± 0.39
	Ga	7.5	5.71 ± 0.44	7.41 ± 0.43	9.98 ± 0.47
	Se	50.0	49.94 ± 1.23	50.90 ± 1.19	52.10 ± 1.20
	Cd	25.0	30.72 ± 0.43	26.61 ± 0.40	19.32 ± 0.36
	In	5.0	4.20 ± 0.36	5.01 ± 0.34	5.98 ± 0.32
70	Cu	12.5	8.93 ± 0.39	9.74 ± 0.39	9.74 ± 0.38
	Ga	8.75	7.17 ± 0.46	7.02 ± 0.46	8.60 ± 0.46
	Se	50.0	50.97 ± 1.29	51.79 ± 1.27	50.81 ± 1.21
	Cd	25.0	29.37 ± 0.43	27.91 ± 0.41	27.83 ± 0.41
	In	3.75	3.57 ± 0.36	3.55 ± 0.35	3.02 ± 0.35
80	Cu	12.5	7.81 ± 0.35	10.22 ± 0.37	10.72 ± 0.39
	Ga	10.0	6.28 ± 0.42	9.93 ± 0.46	10.36 ± 0.49
	Se	50.0	51.58 ± 1.20	50.41 ± 1.17	49.97 ± 1.23
	Cd	25.0	32.67 ± 0.42	27.19 ± 0.39	26.37 ± 0.40
	In	2.5	1.65 ± 0.34	2.25 ± 0.32	2.57 ± 0.33
90	Cu	12.5	1.41 ± 0.30	9.00 ± 0.39	12.67 ± 0.41
	Ga	11.25	1.37 ± 0.38	8.29 ± 0.47	12.39 ± 0.51
	Se	50.0	50.48 ± 1.31	50.46 ± 1.26	51.29 ± 1.22
	Cd	25.0	46.75 ± 0.51	31.49 ± 0.43	23.65 ± 0.39
	In	1.25	0.00	0.76 ± 0.35	0.00

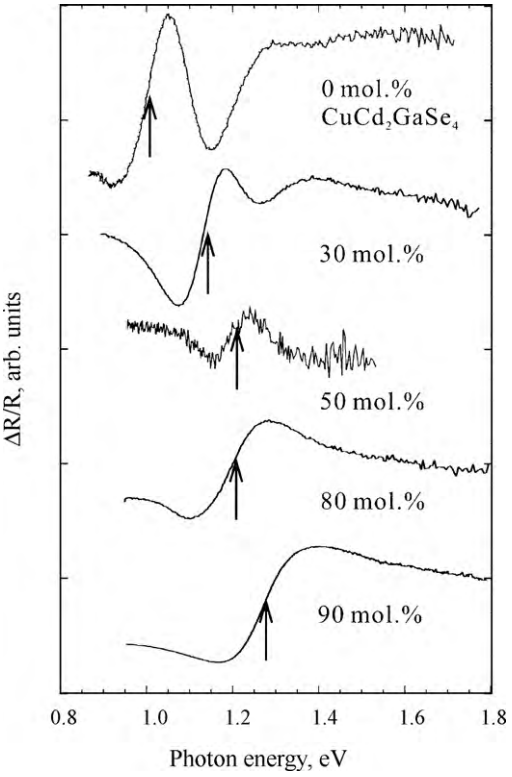

Fig. 12. Photoreflectance spectra for some of the grown γ-solid solution crystals. Arrows indicate the band gap energies estimated from the third derivative approximation.

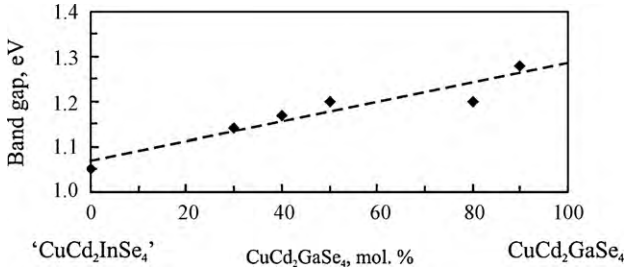

Fig. 13. Variation of the band gap energy with the composition of the γ-solid solution crystals.

'$CuCd_2InSe_4$'–$CuCd_2GaSe_4$ section so that the crystal tip is enriched with CdSe, and the upper part is rich with $CuIn_{1-x}Ga_xSe_2$. Indeed, the Cd content decreases from the ingot tip to the upper part, whereas the Cu and Ga (or In + Ga) content increases, as illustrated by Fig. 11.

Since the composition of the upper part of the crystal is the closest to the tailored composition, the band gap energy is estimated from the PR measurements by focusing the laser on the upper part of the polished crystal plate. Representative photoreflectance spectra are depicted in Fig. 12.

We tentatively assign the observed line shapes to the low-field regime [25], where the band-to-band transition energy can be found from the third derivative. Estimated band gap energies vary almost linearly when substituting In for Ga along the '$CuCd_2InSe_4$'–$CuCd_2GaSe_4$ section (Fig. 13).

4.6. Conclusions

Large region of γ-solid solutions with the sphalerite structure-type was found at 870 K in the $CuInSe_2$–$CuGaSe_2$–2CdSe system; the region is stretched along the '$CuCd_2InSe_4$'–$CuCd_2GaSe_4$ section. Eleven single crystals were grown from the γ-solid solution range using Bridgman method. The band gap energy of the crystals varies from 1.05 eV to ~1.30 eV.

References

[1] A. Goetzberger, C. Hebling, H.-W. Schock, Mater. Sci. Eng. 40 (2003) 1.
[2] R.W. Miles, K.M. Hynes, I. Forbes, Prog. Cryst. Growth Charact. Mater. 51 (2005) 1.
[3] R.W. Miles, K.T. Ramakrishna Reddy, I. Forbes, J. Cryst. Growth 198–199 (1999) 316.
[4] T. Walter, A. Content, K.O. Velthaus, H.W. Schock, Solar Energy Mater. Solar Cells 26 (1992) 357.
[5] J. Djordjevic, C. Pietzker, R. Scheer, J. Phys. Chem. Solids 64 (2003) 1843.
[6] K. Ramanathan, F.S. Hasoon, S. Smith, D.L. Young, M.A. Contreras, P.K. Johnson, A.O. Pudov, J.R. Sites, J. Phys. Chem. Solids 64 (2003) 1495.
[7] V. Probst, J. Palm, S. Visbeck, T. Niesen, R. Tölle, A. Lerchenberger, M. Wendl, H. Vogt, H. Calwer, W. Stetter, F. Karg, Solar Energy Mater Solar Cells 90 (2006) 3115.
[8] Th. Glatzel, H. Steigert, S. Sadewasser, R. Klenk, M.Ch. Lux-Steiner, Thin Solid Films 480–481 (2005) 177.
[9] O.V. Parasyuk, I.D. Olekseyuk, V.I. Zaremba, O.A. Dzham, Z.V. Lavrynyuk, L.V. Piskach, O.G. Yanko, S.V. Volkov, V.I. Pekhnyo, J. Solid State Chem. 179 (2006) 2998.
[10] L.V. Piskach, Z.V. Lavrynyuk, O.V. Parasyuk, O.F. Zmiy, E.M. Kadykalo, V.I. Pekhnyo, S.V. Volkov, Volyn Natl. Univ. Bull. 16 (2008) 47.
[11] L.P. Marushko, L.V. Piskach, Y.E. Romanyuk, O.V. Parasyuk, I.D. Olekseyuk, S.V. Volkov, V.I. Pekhnyo, J. Alloys Compd. 492 (2010) 184.
[12] Y.E. Romanyuk, K.M. Yu, W. Walukiewicz, Z.V. Lavrynyuk, V.I. Pekhnyo, O.V. Parasyuk, Solar Energy Mater. Solar. Cells 92 (2008) 1495.
[13] L. Garbato, P. Manca, Mater. Res. Bull. 9 (1974) 511.
[14] K.O. Dovletov, Ja.A. Khanberdiev, S. Nurev, S.N. Aleksanian, Inorg. Mater. 26 (1990) 939.
[15] I.D. Olekseyuk, E.M. Kadykalo, O.F. Zmiy, Pol. J. Chem. 71 (1997) 893.
[16] L.S. Palatnik, E.K. Belova, Inorg. Mater. 3 (1967) 967.
[17] L.S. Palatnik, E.K. Belova, Inorg. Mater. 3 (1967) 2194.
[18] J.C. Mikkelsen, J. Electron. Mater. 10 (1981) 541.
[19] L. Garbato, F. Ledda, P. Manca, A. Rucci, A. Spiga, Prog. Cryst. Growth Charact. Mater. 10 (1985) 199.
[20] P. Vovk, G. Davydyuk, I. Mishchenko, O. Zmiy, Lviv Natl. Univ. Bull. 39 (2000) 167.
[21] I.D. Olekseyuk, O.V. Parasyuk, O.A. Dzham, L.V. Piskach, J. Solid State Chem. 179 (2006) 315.
[22] I.V. Bodnar, A.P. Bologa, Cryst. Res. Technol. 17 (1982) 339.
[23] K. Yoshino, H. Yokoyama, K. Meada, T. Ikari, J. Cryst. Growth 211 (2000) 476.
[24] F. Paulik, J. Paulik, L. Erdey, System Derivatograph. Theoretical Basis, Hungarian Optical Plant, Budapest, 1974.
[25] F.H. Pollak, H. Shen, Mater. Sci. Eng. A R10 (1993) 275.